Ye Ai[1]
Sang W. Joo[2]
Yingtao Jiang[3]
Xiangchun Xuan[4]
Shizhi Qian[1]

[1]Department of Aerospace Engineering, Old Dominion University, Norfolk, VA, USA
[2]School of Mechanical Engineering, Yeungnam University, Gyongsan, South Korea
[3]Department of Electrical and Computer Engineering, University of Nevada Las Vegas, Las Vegas, NV, USA
[4]Department of Mechanical Engineering, Clemson University, Clemson, SC, USA

Received December 2, 2008
Revised January 14, 2009
Accepted February 3, 2009

Research Article

Transient electrophoretic motion of a charged particle through a converging–diverging microchannel: Effect of direct current-dielectrophoretic force

Transient electrophoretic motion of a charged particle through a converging–diverging microchannel is studied by solving the coupled system of the Navier–Stokes equations for fluid flow and the Laplace equation for electrical field with an arbitrary Lagrangian–Eulerian finite-element method. A spatially non-uniform electric field is induced in the converging–diverging section, which gives rise to a direct current dielectrophoretic (DEP) force in addition to the electrostatic force acting on the charged particle. As a sequence, the symmetry of the particle velocity and trajectory with respect to the throat is broken. We demonstrate that the predicted particle trajectory shifts due to DEP show quantitative agreements with the existing experimental data. Although converging–diverging microchannels can be used for super fast electrophoresis due to the enhancement of the local electric field, it is shown that large particles may be blocked due to the induced DEP force, which thus must be taken into account in the study of electrophoresis in microfluidic devices where non-uniform electric fields are present.

Keywords:
Arbitrary Lagrangian–Eulerian / Dielectrophoresis / Lab-on-a-chip / Microfluidics
DOI 10.1002/elps.200800792

1 Introduction

Electrophoresis has been widely used to characterize, separate, and purify colloids, and to manipulate biological entities such as cells and DNAs in microfluidic as well as many other lab-on-a-chip applications [1, 2]. Numerous studies have thus been performed on the electrophoretic motion of rigid particles in unbounded and confined aqueous electrolyte solutions, as discussed in a recent review by Unni *et al.* [3].

Electrophoresis in converging–diverging microchannels has recently attracted a considerable attention due to its promising applications in super fast electrophoresis [4], sizing and sorting DNA molecules [5], separating beads and biological cells [6–12], focusing particle flows [13], and stretching deformable biological entities, such as individual DNA molecules for genomic analysis [14, 15]. Electric field becomes highly non-uniform in a converging–diverging microchannel, especially when the particle is passing the throat of the converging–diverging section where the cross-sectional area is the minimum. The non-uniform electric field affects the electrostatic force acting on both the particle and the fluid, resulting in significantly different particle motions. In addition, the particle experiences the direct current (DC) dielectrophoretic (DEP) force arising from the interaction between the dielectric particle and the spatially non-uniform electric field. Even in a uniform microchannel, the presence of a particle with a size comparable to the channel cross-section may significantly distort the electric field, yielding a non-trivial DEP force on the particle. For example, Young and Li [16] recently demonstrated that when the gap between a sphere and a channel wall is comparable to the sphere radius, the DEP force should be taken into account when studying the particle motion. However, in most previous numerical studies of particle electrophoresis in non-uniform channels, such as T-shaped [17] and L-shaped microchannels [18], a converging–diverging nanotube [19], and a nanopore connecting two microreservoirs on each side [20], the effects of DEP force have been ignored.

Depending on the electric field and the channel geometry, the induced DEP force may become comparable or even larger than other forces involved, such as electrostatic and hydrodynamic forces, and thus significantly alters the particle electrophoresis. This has been demonstrated through experiments [6–8, 10–13]. In addition, a numerical model based on the Lagrangian tracking method has been developed

Correspondence: Professor Shizhi Qian, Department of Aerospace Engineering, Old Dominion University, ECSB 1309, Elkhorn Avenue, Norfolk, VA 23529-0247, USA
E-mail: sqian@odu.edu
Fax: +1-757-683-3200

Abbreviations: DC, direct current; **DEP,** dielectrophoretic; **EDL,** electric double layer

to understand the DEP effects on particle electrophoresis in microchannels [12]. However, the effects of the particle on the fluid flow and electric fields are both neglected in this model, so is the particle rotation [12]. Instead, a correction factor has to be introduced to account for the particle size effects on the DEP force, and is determined by fitting the numerical predictions to the experimental data.

In the present study, transient electrophoretic motion of a charged particle through a converging–diverging microchannel is numerically investigated for the first time with a full consideration of the particle–fluid–electric field interactions. The induced DEP force is obtained by directly integrating the Maxwell stress tensor over the particle surface without making any assumptions. The structure of this paper is as follows: Section 2 introduces the mathematical model composed of the Navier–Stokes equations for flow field and the Laplace equation for electric field defined in the ALE kinematics. Section 3 describes the numerical method and code validation by comparing the present numerical predictions with a few special cases reported in the literature. The computational results are discussed in Section 4 with focuses on the effect of the DC DEP force, and concluding remarks are given in the ensuing section.

2 Mathematical model

Figure 1A schematically illustrates a charged circular particle of diameter d in a converging–diverging microchannel, which is based on the fabricated device used in the experiment of Xuan *et al.* [8], shown in Fig. 1B. A 2-D Cartesian coordinate system (x, y), with the origin at the center of the throat, is used as shown. The computational domain Ω is surrounded by the channel boundary ABCDEFGHIJ and the particle surface Γ. The segments AJ and EF are, respectively, the inlet and outlet, between which an electric potential difference is applied. The segments ABCDE and FGHIJ are microchannel walls with a uniform zeta potential ζ_w. The particle, with a uniform zeta potential ζ_p on its outer surface Γ, is initially located in the upstream uniform section with a center-to-center distance h off the centerline of the channel. The converging–diverging section is considered to be symmetric with respect to the throat with $L_b = L_c$. The widths of the uniform section and the throat are, respectively, a and b. The length of the upstream uniform section is long enough to ensure a fully developed particle motion prior to the acceleration in the converging section. The particle and microchannel walls are assumed to be rigid and non-conducting. The fluid in the computational domain Ω is incompressible and Newtonian. The effects of Brownian motion and gravity are both ignored.

Compared with the micro-scale channel and particle considered, the electrical double layer (EDL), formed adjacent to the charged surface of particle and channel wall with a typical thickness ranging from 0.1 to 10 nm, is so thin that will not be resolved in detail. Commonly, it will be instead approximated by the Smoluckowski electroosmotic slip

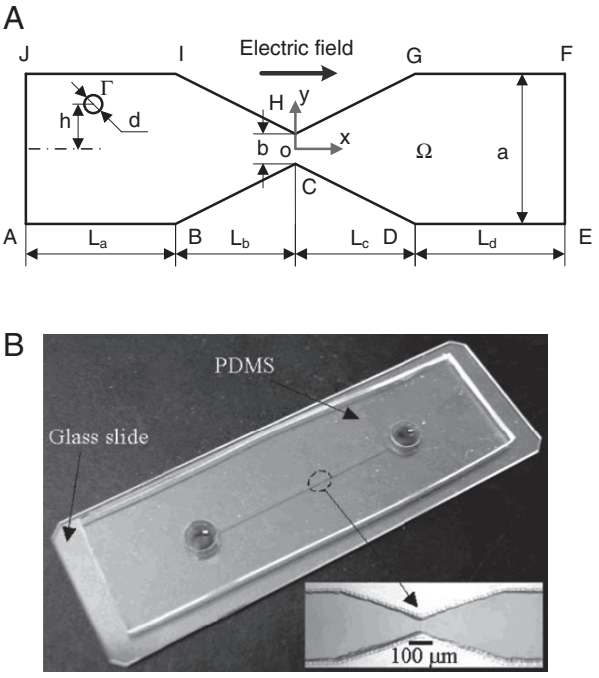

Figure 1. (A) A 2-D schematic view of a circular particle of diameter d and zeta potential ζ_p migrating in a converging–diverging microchannel. The zeta potential ζ_p of the channel wall is ζ_w. An axial electric field, E, is externally applied between the outlet and inlet of the channel; (B) Photograph of a converging–diverging microchannel fabricated with PDMS. The inset shows the converging–diverging section of the microchannel [8].

velocity [17, 18]. In the framework of the thin EDL approximation, the particle and its adjacent EDL are considered as a single entity, and the fluid motion outside the EDL is described by the Stokes equations without any electrostatic body forces. The conservation of mass and momentum in the fluid are thus expressed as

$$\nabla \cdot \mathbf{u} = 0 \quad \text{in } \Omega, \tag{1}$$

and

$$\rho \frac{\partial \mathbf{u}}{\partial t} = -\nabla p + \mu \nabla^2 \mathbf{u} \quad \text{in } \Omega, \tag{2}$$

where $\mathbf{u}$ is the fluid velocity vector, p is the pressure, ρ and μ are, respectively, the fluid density and dynamic viscosity. Since the Reynolds number of electrokinetic flows is usually very small, the inertial terms in the Navier–Stokes equations are neglected.

All the electrokinetic effects induced by the surface charges are incorporated in the Smoluckowski slip velocity boundary conditions. Hence, the fluid velocity adjacent to the channel wall is

$$\mathbf{u} = \frac{\varepsilon \varepsilon_0 \zeta_w}{\mu} (\mathbf{I} - \mathbf{nn}) \cdot \nabla \phi \quad \text{on ABCDE and FGHIJ}, \tag{3}$$

where ε and ε_0 are, respectively, the relative permittivity of the fluid and the permittivity of vacuum, $\mathbf{I}$ is the second-order unit tensor, $\mathbf{n}$ is the unit normal vector pointing from the channel wall to the fluid domain, and ϕ is the electric

potential in the fluid domain. The quantity $(\mathbf{I}-\mathbf{nn})\cdot\nabla\phi$ defines the electric field tangent to the charged channel wall.

Since the particle translates and rotates simultaneously, the boundary condition on the particle surface not only contains the electroosmotic slip velocity but also the translational and rotational velocities of the particle, and is written as

$$\mathbf{u}=\mathbf{U}_\mathrm{p}+\boldsymbol{\omega}_\mathrm{p}\times(\mathbf{x}_\mathrm{s}-\mathbf{x}_\mathrm{p})+\frac{\varepsilon\varepsilon_0\zeta_\mathrm{p}}{\mu}(\mathbf{I}-\mathbf{nn})\cdot\nabla\phi \ \text{ on } \Gamma, \tag{4}$$

where $\mathbf{U_p}$, $\boldsymbol{\omega_p}$, $\mathbf{x_s}$, and $\mathbf{x_p}$ are, respectively, the translational velocity, the rotational velocity, the position vector of the particle surface, and the position vector of the particle center. No pressure gradient is imposed between the inlet AJ and outlet EF.

Due to the assumption of infinitesimal EDL, the net charge density in the computational domain Ω is zero, and so the electrical potential satisfies the Laplace equation

$$\nabla^2\phi=0 \ \text{ in } \Omega. \tag{5}$$

All rigid surfaces are then electrically insulating,

$$\mathbf{n}\cdot\nabla\phi=\mathbf{0} \ \text{ on ABCDE, FGHIJ, and } \Gamma, \tag{6}$$

and the potential difference ϕ_0 applied between the inlet and outlet is imposed by

$$\phi=\phi_0 \ \text{ on EF} \tag{7}$$

and

$$\phi=0 \ \text{ on AJ}. \tag{8}$$

The translational velocity of the particle is governed by the Newton's second law

$$m_\mathrm{p}\frac{\mathrm{d}\mathbf{U}_\mathrm{p}}{\mathrm{d}t}=\mathbf{F}, \tag{9}$$

where m_p is the mass of the particle and $\mathbf{F}$ is the net force acting on it. Since the electrostatic and the hydrodynamic force due to the flow field within the EDL adjacent to the charged particle has the same value but directed in the opposite directions [17], the net force $\mathbf{F}$ is the superposition of the hydrodynamic force, $\mathbf{F_H}$, due to the flow field originated in the outer region of the EDL, and the DC DEP force, $\mathbf{F_{DEP}}$, arising from the interaction between the dielectric particle and the spatially non-uniform electric field:

$$\mathbf{F}=\mathbf{F_H}+\mathbf{F_{DEP}}. \tag{10}$$

Here $\mathbf{F_H}$ and $\mathbf{F_{DEP}}$ are obtained, respectively, by integrating the hydrodynamic stress tensor $\mathbf{T^H}$ and the Maxwell stress tensor $\mathbf{T^E}$ over the particle surface:

$$\mathbf{F_H}=\int\mathbf{T^H}\cdot\mathbf{n}\mathrm{d}\Gamma=\int[-p\mathbf{I}+\mu(\nabla\mathbf{u}+\nabla\mathbf{u}^\mathrm{T})]\cdot\mathbf{n}\mathrm{d}\Gamma \tag{11}$$

and

$$\mathbf{F_{DEP}}=\int\mathbf{T^E}\cdot\mathbf{n}\mathrm{d}\Gamma=\int\left[\varepsilon\varepsilon_0\mathbf{EE}-\frac{1}{2}\varepsilon\varepsilon_0(\mathbf{E}\cdot\mathbf{E})\mathbf{I}\right]\cdot\mathbf{n}\mathrm{d}\Gamma, \tag{12}$$

where $\mathbf{E}$ is electric field related to the electric potential by $\mathbf{E}=-\nabla\phi$. The integration of the first term of the integrand in the right-hand-side of Eq. (12) vanishes due to Eq. (6).

The rotational velocity of the particle is determined by

$$I_\mathrm{p}\frac{\mathrm{d}\boldsymbol{\omega}_\mathrm{p}}{\mathrm{d}t}=\mathbf{Q}=\int(\mathbf{x}_\mathrm{s}-\mathbf{x}_\mathrm{p})\times(\mathbf{T^H}\cdot\mathbf{n})\mathrm{d}\Gamma+\int(\mathbf{x}_\mathrm{s}-\mathbf{x}_\mathrm{p})\times(\mathbf{T^E}\cdot\mathbf{n})\mathrm{d}\Gamma, \tag{13}$$

where I_p is the moment of inertial of the particle and $\mathbf{Q}$ is the torque exerted on the particle.

The center $\mathbf{x_p}$ and the orientation $\boldsymbol{\theta_p}$ of the particle are expressed by

$$\mathbf{x}_\mathrm{p}=\mathbf{x}_\mathrm{p0}+\int_0^t\mathbf{U}_\mathrm{p}\mathrm{d}t \tag{14}$$

and

$$\boldsymbol{\theta}_\mathrm{p}=\boldsymbol{\theta}_\mathrm{p0}+\int_0^t\boldsymbol{\omega}_\mathrm{p}\mathrm{d}t, \tag{15}$$

where $\mathbf{x_{p0}}$ and $\boldsymbol{\theta_{p0}}$ denote, respectively, the initial location and orientation of the particle.

3 Numerical method and code validation

Initially, the fluid velocity and particle velocity are zero, and the particle is positioned in the upstream far away from the converging–diverging section to ensure a steady particle motion prior to arriving at the converging section. The arbitrary Lagrangian–Eulerian (ALE) algorithm, in particular for the simulation of fluid–particle interactions [21, 22], is implemented to track the particle motion in a Lagrangian fashion and at the same time solve the fluid flow and the electric field in an Eulerian framework. Using Eqs. (14) and (15), the ALE algorithm updates the location and the orientation of the particle with deformable mesh after each computational time step. As the particle translates and rotates, the mesh deforms gradually until the mesh quality degrades to a designated level, at which time the integration is forced to stop. Subsequently, the preceding deformed mesh is used to create a new geometry, upon which a new mesh is generated to continue the computation until the next mesh degradation. The ALE algorithm thus can precisely track the whole trajectory of the particle moving through the converging–diverging microchannel.

The coupled system described above is simultaneously solved with a commercial finite-element package COMSOL (version 3.4a, www.comsol.com) operating in a high-performance cluster. The computational domain Ω in Fig. 1A is discretized into quadratic triangular elements with a higher density around the particle and in the channel throat region. We also verified that for the conditions studied here, the numerical solutions are convergent, independent of the size of the elements, and satisfy the various conservation laws.

In order to validate the present computational method and the treatment of the DEP force, we make comparisons

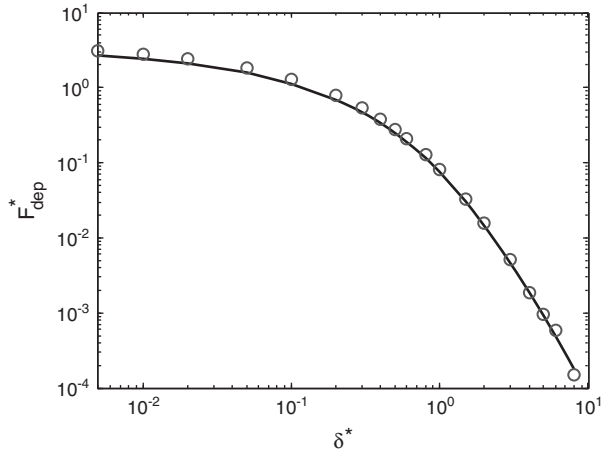

Figure 2. Dimensionless DEP force exerting on a sphere near a planar wall as a function of the dimensionless gap size. The solid line and circles represent, respectively, the analytical solution by Young and Li [16] and our numerical results obtained by a 3-D model.

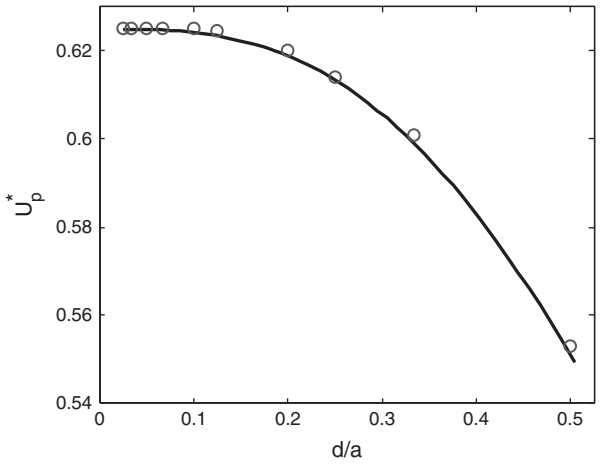

Figure 3. Dimensionless translational velocity of a sphere moving along the axis of a tube as a function of the ratio between the diameter of the sphere and that of the tube. The solid line and circles represent, respectively, the approximation solution from Keh and Anderson [23] and our 3-D numerical results obtained by an axisymmetric model.

with existing analytical and experimental results of electrophoresis in channels with a simple geometry. Figure 2 shows the dimensionless DEP force on a dielectric sphere of radius, r, near a planar wall as a function of the dimensionless gap size, $\delta^* = (d_p - r)/r$, where d_p is the distance from the particle center to the planar wall. The DEP force is normalized by $\varepsilon\varepsilon_0 E_\infty^2 r^2/2$, where E_∞ is the external electric field applied far away from the spherical particle and parallel to the planar wall. Our numerical results (circles) are in good agreement with the ∞ analytical results (solid line) obtained by Young and Li [16].

Figure 3 shows the electrophoretic velocity of a charged spherical particle of diameter d translating along the axis of an infinitely long tube of diameter a. The approximate solution, valid for thin EDL and absence of DEP force,

$$U_p^* = \left[1 - 1.28987\left(\frac{d}{a}\right)^3 + 1.89632\left(\frac{d}{a}\right)^5 - 1.02780\left(\frac{d}{a}\right)^6 + O\left(\left(\frac{d}{a}\right)^8\right)\right](1-\gamma), \quad (16)$$

was derived by Keh and Anderson [23], where $\gamma = \zeta_w/\zeta_p$ denotes the ratio of the zeta potential ζ_p of the particle to that of the channel wall. The translational velocity of the particle is normalized by $\varepsilon\varepsilon_0\zeta_p E_{z/\mu}$ with E_z representing the electric field along the axis of the tube in the absence of the particle. The present numerical results (circles) show good agreement with the approximate solution (solid line), in which the DEP force does not affect the particle motion due to axial symmetry.

Another validation of the present method is performed for the electrophoretic motion of a charged circular particle in a straight microchannel with a rectangular hurdle in the middle, as shown in Fig. 4. The present numerical results are compared against the experimental data obtained by Kang *et al.* [12]. As in the converging–diverging microchannel, a spatially non-uniform electric field is induced by

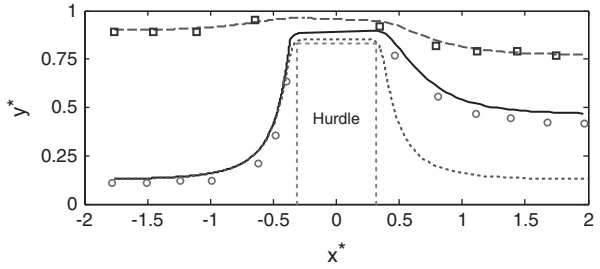

Figure 4. Particle trajectories through a microchannel with a rectangular hurdle in the middle. The solid and dashed lines represent the predicted particle trajectories with considering the DEP force, the circles, and squares represent the experimental data obtained by Kang *et al.* [12], and the dotted line represents the predicted particle trajectory of the lower particle without considering the DEP force. The x and y locations are both normalized by the channel width.

the hurdle, and DC DEP force is generated. The experiments demonstrate that the trajectory of particles close to the lower wall is strongly asymmetric with respect to the hurdle, resulting in conspicuous shift toward the upper wall after passing the hurdle. For two 15.7 μm particles under a 20 kV/m electric field shown, our numerical predictions (solid and dashed lines) are in good agreement with the experimental data (symbols). If the DEP force were neglected, the predicted particle trajectory (dotted line) would be symmetric with respect to the hurdle, with substantial discrepancy with the experimental data. It can be concluded that the trajectory shift is attributed to the DEP force, which must be taken into account for the electrophoretic motion of particles in microchannels with non-uniform cross-sections, such as converging–diverging microchannels, where the electric field is non-uniform.

4 Results and discussion

Using the computational method developed, a comprehensive parametric study has been performed to understand the DEP force in a converging–diverging microchannel. In this section, discussions on a few representative cases are provided in dimensional terms with focus on the effects of the electric field and particle size on the particle velocity and trajectory. The lengths of the symmetric converging–diverging section are taken from the fabricated device of Xuan *et al.* [8] with $L_b = L_c = 400\,\mu m$, whereas that of the entire microchannel is set to 1500 μm, with $L_a = 400\,\mu m$ and $L_d = 300\,\mu m$. The widths of the uniform section and throat are, respectively, $a = 325\,\mu m$ and $b = 55\,\mu m$. The applied electric field strength E is calculated by dividing the electric potential difference between the inlet and outlet over the total length of the microchannel. The initial transverse location of the particle is defined as the ratio of the initial distance between the particle center and the channel centerline to the half width of the straight section, $h^* = 2h/a$.

4.1 Trajectory shift

Figure 5A shows the predicted particle trajectories through a converging–diverging microchannel in the presence (solid and dashed lines) and absence (circles and squares) of the DEP force when $E = 10$ KV/m, $d = 20\,\mu m$, $\zeta_p = 58$ mV, and $\gamma = 0.3$. The solid line (or circles) and dashed line (or squares) correspond, respectively, to $h^* = -0.5$ and $h^* = 0.7$. It is clearly seen that the particle trajectory becomes asymmetric with respect to the channel throat when the DEP force is considered. After passing through the throat, particles are pushed toward the centerline of the channel, which will be explained below. In Fig. 5B the predicted particle trajectories are compared with the experimental results (symbols) when $E = 15$ KV/m, $d = 10.35\,\mu m$, $\zeta_p = -32$ mV, and $\gamma = 2.5$. Note that the particle size in Fig. 5B is smaller than that in Fig. 5A. Since the DEP force is proportional to the particle size, the particle in Fig. 5B experiences a slighter trajectory shift than that in Fig. 5A due to a smaller induced DEP force. The size-dependent separation demonstrated in [6, 7, 10–12, 24] is based on the idea that particles with different sizes experience different trajectory shifts due to the particle-size-dependence of the DEP force.

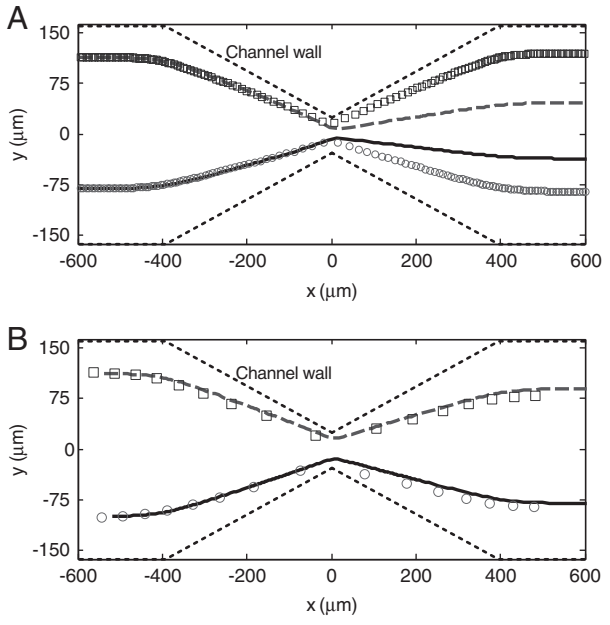

Figure 5. (a) Predicted particle trajectories with (solid and dashed lines) and without (circles and squares) considering the DEP force. $E = 10$ KV/m, $d = 20\,\mu m$, $\zeta_p = 58$ mV, $a = 325\,\mu m$, $b = 55\,\mu m$, and $\gamma = 0.3$. (b) Predicted particle trajectories with considering the DEP force (solid and dashed lines) compared with the experimental data (circles and squares). $E = 15$ KV/m, $d = 10.35\,\mu m$, $\zeta_p = -32$ mV, $a = 325\,\mu m$, $b = 55\,\mu m$, and $\gamma = 2.5$.

Figure 6 shows the distribution of the DEP force near the throat obtained by a point-dipole approximation [25] without considering the effect of the particle on the electric field. The color levels in Fig. 6 represent the dimensionless electric field strength, which is normalized by $2\phi_0/d$. As the particle experiences a negative dielectrophoresis, the DEP force acting on the particle always points to the region of a lower electric field. Since the maximum electric field strength occurs at the throat, the DEP force is directed away from it, as shown in Fig. 6. The trajectory (a) shown in Fig. 6 represents the predicted particle trajectory without considering the DEP force, which is identical to the streamline of the flow field originated from the initial location of the particle. The x-component of the DEP force is negative in the converging section and becomes positive in the diverging section. The y-component DEP force is negative (positive) in the region above (below) the centerline of the

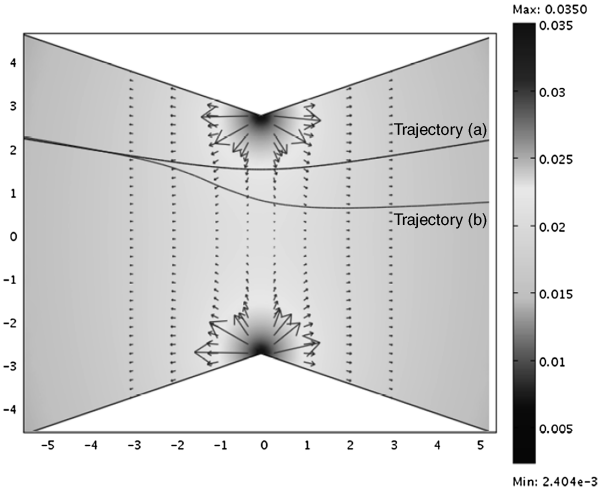

Figure 6. Distribution of the DEP force (arrows) around the throat of the converging–diverging microchannel. The color levels represent the normalized electric field strength. The trajectories (a) and (b) represent, respectively, the predicted particle trajectories without and with considering the DEP force.

microchannel. Away from the converging–diverging section, the DEP force gradually decays, and becomes negligible in the uniform section of the channel. When a particle is initially located above the centerline and electrophoretically migrates to the converging section, the particle experiences negative *x*-component and *y*-component DEP forces, which push the particle toward the centerline of the channel. After it passes the throat, the *x*-component DEP force becomes positive, whereas the *y*-component DEP force is still negative. The positive *x*-component DEP force accelerates the translation of the particle, whereas the negative *y*-component DEP force continues to push the particle toward the centerline of the channel. Particles transported along the centerline of the channel would not experience the trajectory shift.

4.2 Effect of electric field

Several different electric fields are applied to drive the electrophoretic motion of a 20-μm particle moving along the centerline of the converging–diverging microchannel with $\zeta_p = -32$ mV, and $\gamma = 2.5$. Figure 7A shows the ratio of the translational velocity of the particle to that in the uniform upstream section, $\lambda_p = U_p/U_{up}$, under the electric field of 10 KV/m (solid line), 20 KV/m (dotted line), and 35 KV/m (dash–dotted line), respectively. For comparison, the translational velocity ratio without considering the DEP force is also shown in Fig. 7A (dashed line), which as expected is symmetry with respect to the throat and independence of the electric field. When the DEP force is taken into account, however, the translational velocity ratio is asymmetric with respect to the throat and strongly dependent of the electric field applied. This is because that the *x*-component DEP force is negative in the converging section, whereas positive in the diverging section, as shown in Fig. 6.

To clearly explain the asymmetric velocity ratio profile and its dependence of the electric field, we analyze the electrophoretic and DEP forces acting on a particle along the centerline of the channel. For the electrophoretic motion of a sphere with a radius of 10 μm and density of 1000 kg/m^3, the characteristic time for reaching a steady translational velocity is in the order of 10^{-4} s. The variation of the particle's translational velocity generally follows a similar trend of the electrokinetic force exerted on the particle [12]. Due to the thin EDL approximation, the electrophoretic force is not explicitly solved in the present model. We instead estimate the dimensional electrophoretic force acting on a sphere of radius *r* as [26]

$$\mathbf{F_{EP}} = (\gamma - 1)6\pi\zeta_p\varepsilon\varepsilon_0 r\mathbf{E}. \quad (17)$$

The dimensional DEP force acting on the particle is given by Eq. (12), which reveals the quadratic dependence of the DEP force on the electric field, in contrast to the linear dependence of the electrophoretic force. For high electric fields the DEP force can dominate. Figure 8 shows the normalized electrophoretic force (dash–dotted line), DEP force (dashed line) and superposition of the two forces (solid line) acting on the particle along the centerline of the channel under an electric field of 15 KV/m. The forces are normalized by $\varepsilon\varepsilon_0\zeta_p\phi_0$. The electrophoretic force is symmetric about the throat with the maximum occurring at the throat. The DEP force is insignificant in the uniform sections, but becomes important near the throat. As the negative DEP force always points to the region of a lower electric field, the direction of the DEP force in the upstream is opposite to that in the downstream, as is also shown in Fig. 6, which retards the particle motion in the converging section but accelerates it in the diverging section. The translational velocity ratio in the converging section is lower than that in the absence of

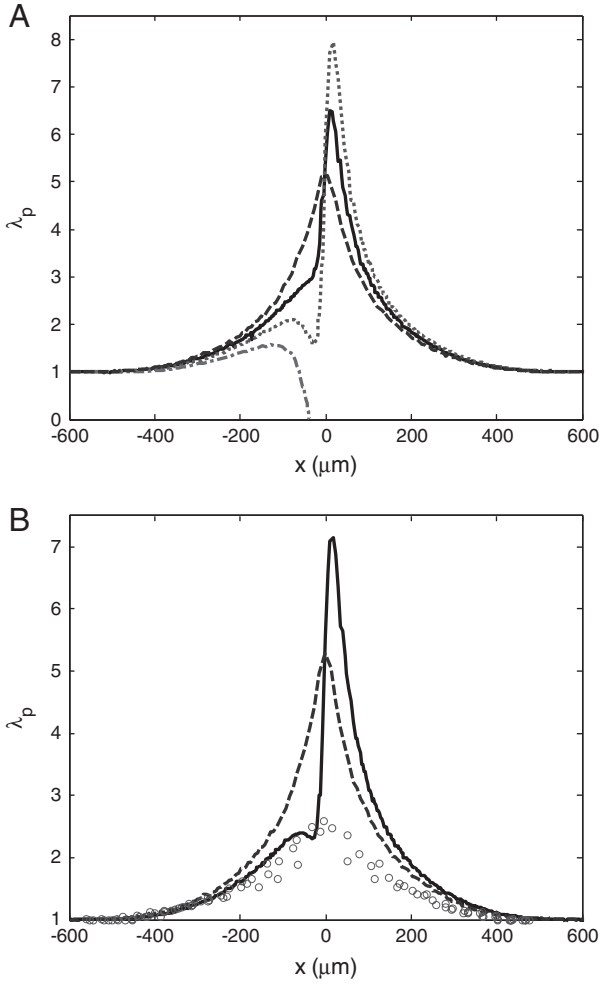

Figure 7. (A) Translational velocity ratio of a 20-μm particle along the centerline of the converging–diverging microchannel. $\zeta_p = -32$ mV, $a = 325$ μm, $b = 55$ μm, and $\gamma = 2.5$. The solid, dotted, and dash–dotted lines represent, respectively, the velocity ratio under an electric field of $E = 10$, 20, and 35 KV/m with considering the DEP force. The symmetric dashed line represents the velocity ratio without considering the DEP force. (B) The velocity ratio under an electric field of 15 KV/m. The solid line, dashed line (symmetric), and circles represent, respectively, the numerical prediction with considering the DEP force, numerical prediction without considering the DEP force, and the experimental data obtained by Xuan *et al.* [8].

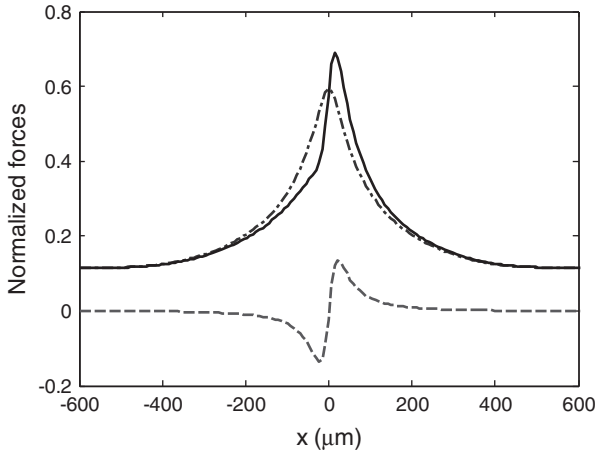

Figure 8. Normalized electrokinetic forces acting on a 20-μm particle under an electric field of 15 KV/m. Dashed, dash–dotted, and solid lines represent, respectively, the DEP force, electrophoretic force, and the superposed electrokinetic force. $\zeta_p = -32$ mV, $a = 325$ μm, $b = 55$ μm, and $\gamma = 2.5$.

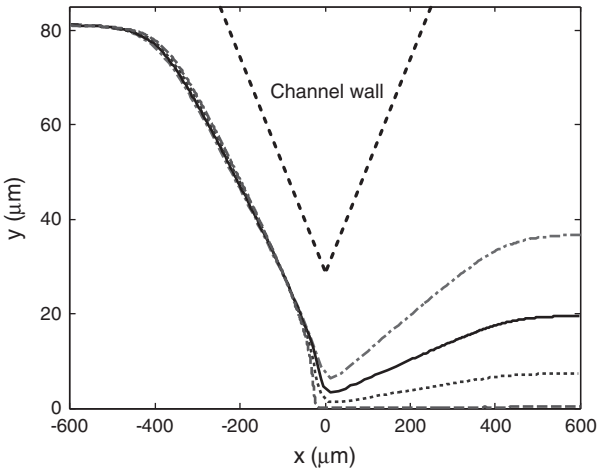

Figure 9. Particle trajectories of a 20-μm particle initially located at $h^* = 0.5$ under electric fields of $E = 10$ KV/m (dash–dotted line), $E = 15$ KV/m (solid line), $E = 20$ KV/m (dotted line), and $E = 25$ KV/m (dashed line). $\zeta_p = 58$ mV, $a = 325$ μm, $b = 55$ μm, and $\gamma = 0.3$.

the DEP force, as shown in Fig. 7A. However, the translational velocity ratio in the diverging section is higher than that with no DEP force. When the particle is located exactly at the center of the throat, the surrounding electric field is symmetric with respect to the particle center, and so the net DEP force vanishes. Thus, the translational velocity ratio at the throat predicted either with considering the DEP force or not is the same. The maximum translational velocity ratio occurs in the diverging section where the DEP force (dashed line in Fig. 8) and thus the superposition of the electrostatic and DEP forces (solid line) reaches a maximum. Although the cross-sectional area ratio of the uniform section to the throat is 5.91, the maximum translational velocity ratio with the DEP force can easily exceed this value. When the electric field is above a critical value, the negative *x*-component DEP force in the converging section becomes large enough to prevent the particle from passing the throat (dash–dotted line in Fig. 7A), which is also observed experimentally by Kang *et al.* [12].

Figure 7B shows the comparison of the numerically predicted translational velocity ratios (lines) with the experimental data (symbols) obtained by Xuan *et al.* [8] under an electric field of 15 KV/m. The solid and dashed lines represent, respectively, the predictions with and without the DEP force. In the converging section, the numerical results with the DEP force (solid line) are in good agreement with the experimental data. However, considerable disagreement is seen in the diverging section. The experimental data seem almost symmetric, and do not show the peak just after the throat. The main reason that a clear DEP effect on the velocity ratio was not observed in the experiments appears to be difficulties in the measurement. Particles move fast near the channel throat while the camera used can take images at only 15 frames *per* second, resulting in at most a couple of data points for each particle in the throat region. With these few data, it is hard to tell whether the particle velocity ratio is symmetric or asymmetric about the channel throat from the experimental data alone. Only when the DEP effect is strong enough, which is not the case in the experimental conditions used, the asymmetric profile can be clearly observed.

Figure 9 shows the particle trajectory shift due to the DEP force under four different electric fields when $d = 20$ μm, $h^* = 0.5$, $\zeta_p = 58$ mV, and $\gamma = 0.3$. A higher electric field leads to a larger trajectory shift. In the case of $E = 25$ KV/m, the particle is shifted to the centerline of the channel after passing the throat. It is thus noted that the converging–diverging channels can be used for particle focusing, which has been observed experimentally by Xuan *et al.* [27] and also successfully implemented by Thwar *et al.* [13] in a straight channel with a pair of oil menisci.

4.3 Effect of particle size

Figure 10 shows the translational velocity ratio of particles with different sizes along the centerline of the channel when $\zeta_p = 58$ mV and $\gamma = 0.3$. As discussed above, the DEP force exerted on a spherical particle varies with the cubic of its radius. Therefore, the DEP force diminishes fairly rapidly with the decrease in particle size. For example, the translational velocity ratios for a 10-μm particle with (solid line) and without (dashed line) the DEP force are very close, as shown in Fig. 10. As the particle size increases to 25 μm, the resulting DEP force becomes large enough to establish a clearly asymmetric particle motion with respect to the throat (dotted line). For even larger particles, the DEP force can prevent the particle from passing through the throat, which indicates that the converging–diverging microchannels may be used for particle trapping and sorting.

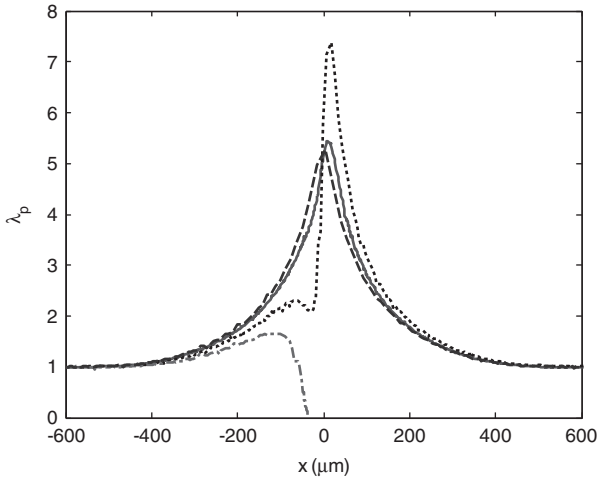

Figure 10. Translational velocity ratio of particles with diameter $d = 10\,\mu m$ (solid line), $d = 25\,\mu m$ (dotted line), and $d = 40\,\mu m$ (dash–dotted line) along the centerline of the converging–diverging microchannel under an electric field of 10 KV/m. The symmetric dashed line represents the predicted velocity ratio of a 20 μm particle without considering the DEP force. $\zeta_p = 58$ mV, $a = 325\,\mu m$, $b = 55\,\mu m$, and $\gamma = 0.3$.

5 Concluding remarks

The effect of DEP force, arising from a non-uniform electric field, on the electrophoretic motion of particles through a converging–diverging microchannel is numerically investigated for the first time using a transient ALE finite element model. We demonstrate that the particle velocity along the converging–diverging microchannel, which is symmetric with respect to the throat when the DEP effect is neglected, becomes asymmetric due to the opposite directions of the DEP forces induced in the converging and diverging sections. For larger particles or electric fields, the DEP force may be strong enough to prevent the particles from passing through the microchannel, which may be used for particle trapping and sorting. Particles initially located away from the centerline of the channel experience trajectory shift toward the centerline in the downstream, which is in good agreement with existing experimental data and shows applicability to particle focusing. As particles with different sizes experience different trajectory shifts, converging–diverging microchannels have a great potential for continuous separation of biological entities like cells and DNAs, which has been demonstrated in several experimental works.

This work was supported, in part, by the Korea Research Foundation Grant KRF-2008-313-D00117 funded by the Korean Government (SWJ) and UNLV PRA (YJ).

The authors have declared no conflict of interest.

6 References

[1] Hunter, R. J., *Foundations of Colloid Science*. Oxford University Press, New York, 2001.

[2] Li, D., *Electrokinetics in Microfluidics*. Elsevier Academic Press, New York, 2004.

[3] Unni, H. N., Keh, H. J., Yang, C., *Electrophoresis* 2007, *28*, 658–664.

[4] Plenert, M. L., Shear, J. B., *Proc. Natl. Acad. Sci. USA* 2003, *100*, 3853–3857.

[5] Chou, H. P., Spence, C., Scherer, A., Quake, S., *Proc. Natl. Acad. Sci. USA* 1999, *96*, 11–13.

[6] Barbulovic-Nad, I., Xuan, X. C., Lee, J. S. H., Li, D., *Lab Chip* 2006, *6*, 274–279.

[7] Kang, Y. J., Li, D., Kalams, S. A., Eid, J. E., *Biomed. Microdevices* 2008, *10*, 243–249.

[8] Xuan, X. C., Xu, B., Li, D., *Anal. Chem.* 2005, *77*, 4323–4328.

[9] Xuan, X. C., Li, D., *J. Micromech. Microeng.* 2006, *16*, 62–69.

[10] Kang, K. H., Kang, Y. J., Xuan, X. C., Li, D., *Electrophoresis* 2006, *27*, 694–702.

[11] Lewpiriyawong, N., Yang, C., Lam, Y. C., *Biomicrofluidics* 2008, *2*, 034105.

[12] Kang, K. H., Xuan, X. C., Kang, Y. J., Li, D., *J. Appl. Phys.* 2006, *99*, 064702.

[13] Thwar, P. K., Linderman, J. J., Burns, M. A., *Electrophoresis* 2007, *28*, 4572–4581.

[14] Larson, J. W., Yantz, G. R., Zhong, Q., Charnas, R., D'Antoni, C. M, Gallo, M. V., Gillis, K. A. *et al.*, *Lab Chip* 2006, *6*, 1187–1199.

[15] Hsieh, S. S., Liou, J. H., *Biotechnol. Appl. Biochem.* 2008, 18251714.

[16] Young, E. W. K., Li, D., *Langmuir* 2005, *21*, 12037–12046.

[17] Ye, C. Z., Li, D., *J. Colloid Interface Sci.* 2004, *272*, 480–488.

[18] Davison, S. M., Sharp, K. V., *Microfluid Nanofluid.* 2008, *4*, 409–418.

[19] Qian, S., Wang, A. H., Afonien, J. K., *J. Colloid Interface Sci.* 2006, *303*, 579–592.

[20] Liu, H., Qian, S., Bau, H. H., *Biophys. J.* 2007, *92*, 1164–1177.

[21] Hu, H. H., Joseph, D. D., Crochet, M. J., *Theor. Comput. Fluid Dyn.* 1992, *3*, 285–306.

[22] Hu, H. H., Patankar, N. A., Zhu, M. Y., *J. Comput. Phys.* 2001, *169*, 427–462.

[23] Keh, H. J., Anderson, J. L., *J. Fluid Mech.* 1985, *153*, 417–439.

[24] Parikesit, G. O. F., Markesteijn, A. P., Piciu, O. M., Bossche, A., Westerweel, J., Young, I. T., Garini, Y. *et al.*, *Biomicrofluidics* 2008, *2*, 024103.

[25] Pohl, H. A., *Dielectrophoresis*. Cambridge University Press, Cambridge, UK, 1978.

[26] Probstein, R. F., *Physicochemical Hydrodynamics* Wiley, New York, 1994.

[27] Xuan, X. C., Raghibizadeh, R., Li, D., *J. Colloid Interface Sci.* 2005, *296*, 743–748.

